Development of a spin polarized low energy electron diffraction system

A. V. Pradeep,[1] Arnab Roy,[1] P. S. Anil Kumar,[1] and J. Kirschner[2]
[1]*Department of Physics, Indian Institute of Science, Bangalore 560012, India*
[2]*Max-Planck-Institut für Mikrostrukturphysik, Weinberg 2, D-06120 Halle (Saale), Germany*

(Received 18 July 2015; accepted 24 January 2016; published online 18 February 2016)

We have designed and constructed a spin polarized low energy electron diffraction system working in the reflected electron pulse counting mode. This system is capable of measuring asymmetries due to spin-orbit and exchange interactions. Photoemission from a strained GaAs/GaAsP super lattice is used as the source of spin polarized electrons. Spin-orbit asymmetry is evaluated for Ir(100) single crystal at various energies. Subsequently, exchange asymmetry has been evaluated on 40 monolayer Fe deposited on Ir(100). This instrument proves to be useful in understanding structure and magnetism at surfaces. © *2016 AIP Publishing LLC.* [http://dx.doi.org/10.1063/1.4941682]

I. INTRODUCTION

Spin polarized electron beam has not yet been produced from an unpolarized electron beam using Stern-Gerlach type spin filter, because of the Lorentz force and Heisenberg uncertainty principle,[1–3] even though there are predictions that with longitudinal magnetic field gradient one can achieve this.[3] At present, electron spin detectors and filters work on the basis of spin dependent scattering of electron beam from crystal surfaces. The spin dependent contribution in the electron solid interaction Hamiltonian comes from spin-orbit (S-O) interaction (from high Z materials) and exchange interaction (from ferromagnetic materials). There exists spin filters in the high energy side (Mott scattering from high Z material and Moller scattering from ferromagnetic materials) as well as low energy side (spin polarized low energy electron diffraction (SPLEED) detectors).[4–9] Mott detector is a widely used spin detector that makes use of the difference in intensity of equivalent diffracted beam. They work in the higher energy range, which is around 100 keV, and suffer from low figure of merit of the order of 10^{-4}, whereas SPLEED based detectors make use of the normalised difference in the intensities of specularly reflected beam between an incident spin up and spin down electron beam, and work in the lower energy range within 100 eV. Even though their figure of merit, which is of the order of 10^{-3} to 10^{-2}, is far better than that of Mott detector,[10,11] it is important to find new materials that have higher efficiency and long lifetime.[12] In addition, SPLEED system allows us to study the spin-orbit and exchange scattering at crystal surfaces. Hence, both, for fundamental studying and technological applications, SPLEED will be valuable technique.[13–16] In this paper, we describe the assembly and successful testing of a new SPLEED system.

The most important part of a SPLEED system is the beam of spin polarized electrons whose spin orientation and energy can be controlled. We use photoemission from a strained GaAs/GaAsP super lattice photocathode as the spin polarized electron beam.[17] They have high polarization when compared to normal GaAs.[18–20] A microchannel plate (MCP), that is capable of detecting even a single electron, is used as the electron detector. To get the spin polarized beam, the photocathode needs to be activated by making the surface a negative electron affinity (NEA) surface. This is done by depositing caesium (Cs) and oxidising it in a sequential manner (Yo-Yo process).[19–21] We use single crystal Ir(100) and iron film grown on Ir(100) as scattering targets. Since the penetration depth of low energy (20 eV to 100 eV) electron beam is about 5-10 Å, the surface cleanliness is very important. The surface contamination and crystal quality are monitored by Auger electron spectroscopy (AES) and low energy electron diffraction (LEED). Iron films are grown on iridium by using electron beam (e-beam) evaporation, and the growth is monitored by medium energy electron diffraction (MEED) oscillations. Entire experiment is done in ultrahigh vacuum (UHV).

II. INSTRUMENT

The instrument consists of two UHV μ-metal chambers connected through a gate valve. In the first chamber (hereafter called source chamber), spin polarized electrons are created. Electrons are ejected out of the photocathode (discussed in Section III) with their spin angular momentum parallel (antiparallel) to the propagation direction. They are deflected through 90° using a static electric field to make the spin angular momentum perpendicular to the direction of propagation. Then they are focussed onto the target by a set of electrostatic lenses over a distance of 46 cm through 2 mm diameter aperture. In the second chamber (hereafter called scattering chamber), the scattering target (Ir(100)), LEED, AES, e-beam evaporator, quadrupole mass spectrometer, and electron detectors are installed. Scattering experiments are done in this chamber. Single crystal Ir(100) is mounted on an electrically isolated target holder from the top of the scattering chamber that can rotate about its axis and also having x, y, and z motion. A tungsten filament is mounted behind the sample for heating. A thermocouple attached to the sample holder measures the temperature. Fig. 1 shows the scattering chamber configuration.

Electron detector is a MCP mounted on the arm of the detector holder and is attached from the bottom of the scattering chamber. The detector can move around the sample on a cylindrical surface of radius 8 cm as well as it has an X, Y, and

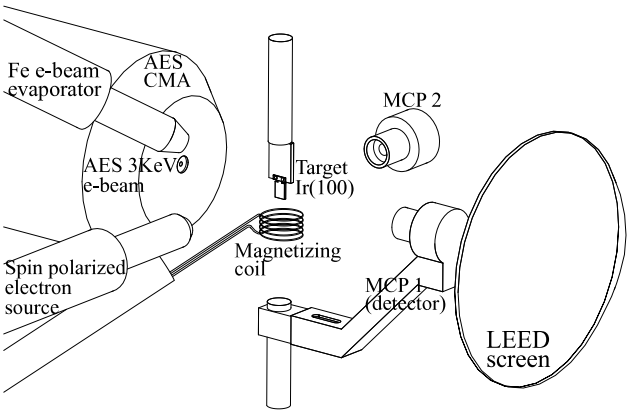

FIG. 1. Schematics of the SPLEED scattering chamber. Scattering target Ir(100) (rotatable) is kept at the focal point of spin polarized electron source, e-beam evaporator, and AES cylindrical mirror energy analyser. A magnetizing coil is kept below the target. MCP1 (rotatable) is used for detecting specularly reflected electron and MCP2 (fixed) is used for detecting direct electron from the spin polarized electron source. LEED screen, installed diametrically opposite to the AES-CMA, is also shown.

Z motion. Detector has an acceptance area of diameter 5 mm. In order to filter the in-elastically scattered electrons, a grid is placed in front of the detector. The grid is kept at 5 V with respect to the cathode potential, which determines the energy of the electron beam, to reject the electron with energy loss more than 5 eV. AES and LEED are kept diametrically opposite to each other. So 180° sample rotation about its axis allows us to move the sample from LEED operating point to AES operating point. Source chamber is pumped by a 550 l/s turbo molecular pump, 160 l/s getter ion pump and a titanium sublimation pump (TSP), and the base vacuum is $\sim 3 \times 10^{-11}$ mbar. Scattering chamber is pumped by a 550 l/s turbo molecular pump, 320 l/s getter ion pump and a TSP, and the base vacuum is $\sim 5 \times 10^{-11}$ mbar. Ion pump, Ion gauge, and quadrupole mass spectrometer are kept far from the scattering point in order to avoid the deflection of electron beam by the magnetic field produced by ion pump and stray electrons from the filaments of these components. The e-beam evaporator is installed through a 2.75 in. flange. AES, LEED, spin polarized electron gun, electron detector, and e-beam evaporator are arranged in such a way that the Ir(100) crystal comes at the focal point of all these components. In addition, a retractable five turn coil of diameter 25 mm is installed in order to magnetize the Fe film. Leak valves are connected to the source chamber as well as scattering chamber for giving controlled leak of ultrahigh pure (UHP) oxygen and hydrogen.

III. SPIN POLARIZED ELECTRON SOURCE

Figure 2 shows an overall view of spin polarized electron gun. Photocathode is mounted on top of an isolated thin metal plate to which a thermocouple is spot welded. A negative voltage applied to this plate with respect to the grounded sample determines the energy of the electron beam. Prior to the activation, the photocathode has to be degassed and cleaned by heating in a controlled manner. For this a tungsten filament is mounted under the above mentioned metal plate. Cs dispenser is mounted on the electrostatic lens V_1.

A. Cathode activation

Photocathode is a strained GaAs/GaAsP super lattice.[17] This photocathode, with a thin arsenic coating in order to protect from atmospheric oxidation, was installed in the system. Temperature of the cathode was increased slowly by means of radiative heating from the filament kept below the cathode in 30 min. The cathode is kept at 410 °C for 50 min for degassing the surrounding and for removing the arsenic capping and slowly ramped down to room temperature. Then cathode was degassed by flashing up to 430 °C in 2 min.[22] Flash degassing avoids the degassing of the surroundings and only degasses the cathode. During these processes, all the focussing voltages are switched off and the cathode is grounded.

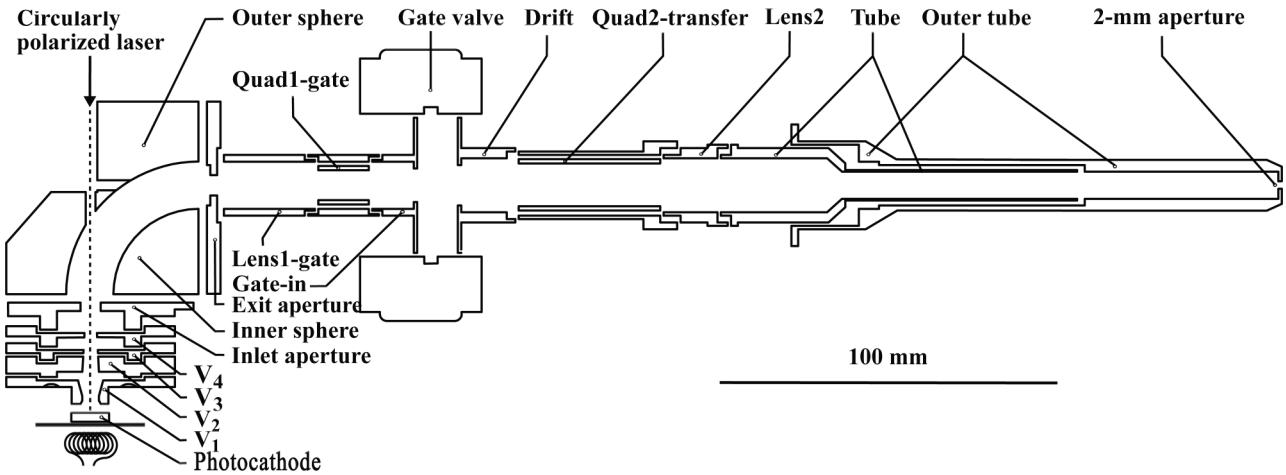

FIG. 2. Spin polarized electron gun. V_1, V_2, V_3, and V_4 are the electrostatic lenses placed just above the photocathode. Circularly polarized laser, shown as dotted lines, enters to the cathode through a hole drilled into the outer sphere of the 90° deflector. Inlet and exit aperture are kept at potential called pass energy. A negative potential is given to outer-sphere and a positive potential is given to inner-sphere, with respect to pass energy, to deflect the beam. Quad1-gate and quad2-transfer are two sets of quad plate used for deflecting the beam. Lens1-gate, gate-in, drift, lens2, and tube are electrostatic lenses used for focusing. A gate valve, for isolating two chambers, is inserted between gate-in and drift. The outer tube is kept at a ground potential to make field free region inside the scattering chamber.

The surface of the photocathode is made a NEA surface by depositing Cs and oxidising it in a sequential manner. Cs is deposited from a dispenser by passing current through it. To avoid desorption of Cs from the cathode at an elevated temperature, initially the Cs dispenser is kept off until the photocathode temperature goes below 60 °C. The photocathode is grounded through an electrometer to measure the photocurrent. A diode laser of wavelength 632 nm is focussed on to the photocathode for photoemission and the voltages at V_1, V_2, and V_3 are kept at 35 V to extract the photoelectrons. The Cs dispenser is activated by passing a current of 3.6 A through the dispenser. Then, the photocurrent increases and goes through a maximum and starts falling down. At this point, the Cs flux is reduced and UHP oxygen is introduced so that the pressure in the chamber rises to 5×10^{-9} mbar (without any additional ion gauge correction for oxygen), then the photocurrent increases and goes through a maximum and the leak valve is closed when the photocurrent starts falling down. Then the Cs oven is again activated. This cycle is repeated 5–10 times to get a good photocurrent.[21] Fig. 3 shows the activation process. At the end of activation process, the Cs dispenser is kept at a standby current to stabilize the photocurrent.[23] Then, the diode laser of wavelength 632 nm is kept off and the photocathode is connected to a negative voltage source with respect to the sample which determines the energy of the electron beam. The life time of this cathode is about one week. After this time, the cathode has to be regenerated again.

B. Excitation of spin polarized electron

Spin polarized electrons are created by shining the activated photocathode with a circularly polarized light of wavelength 830 nm. We use commercially available laser diode of wavelength 830 nm and a polarization-maintaining and single mode optical fiber. By changing the polarization from left circularly polarized (σ^-) to right circularly polarized (σ^+) light, we can change the electron spin angular momentum from spin up to spin down. For which, a linearly polarized light of wavelength 830 nm is passed through liquid crystal polarization rotator and a quarter wave plate. By applying a suitable ac voltage (6.975 V and 2.366 V) to the liquid crystal polarization rotator, the linear polarization of the light can be switched from +45° to −45° with respect to the optical axis of the quarter wave plate which will give σ^+ and σ^- circularly polarized light, respectively. The photocathode is shined by this light through a polarization maintaining view port and through a hole drilled on the 90° deflector as shown in Fig. 2. This gives a spin polarized electron beam with spin angular momentum parallel (antiparallel) to the direction of propagation.

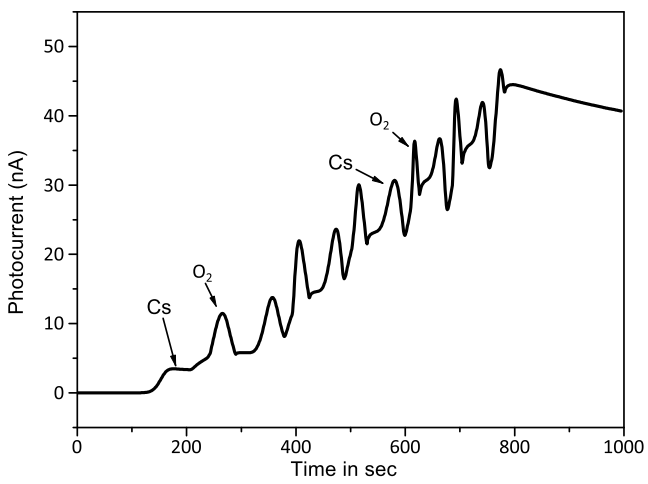

FIG. 3. Photocurrent vs time plot during photocathode activation process. During Cs deposition the photocurrent increases, goes through maxima, and then decreases. This is shown as Cs peak. When oxygen is introduced, the photocurrent peaks up and decreases when the oxygen is excess. This is shown as O_2 peak.

C. Focussing

The spin angular momentum of the electron beam should be made perpendicular to its direction of propagation to get maximum asymmetry. This is because the asymmetry vector lies perpendicular to the scattering plane, which is defined by incident electron beam wave vector and surface normal. In Fig. 2, V_1, V_2, V_3, and V_4 are lenses that extract the electrons from the photocathode. Pass energy is the positive voltage applied to the inlet and exit aperture of the 90° deflector. Outer sphere of the deflector is kept at a negative voltage and the inner sphere is kept at a positive voltage with respect to the pass energy. This static electric field deflects the direction of propagation of electron beam through 90° on the other hand it does not alter the spin angular momentum. In other words, the longitudinal spin of the electron beam is changed to transverse spin. For a well defined wave vector, the electron beam has to be collimated and focussed onto the sample. In order to do this, different dc voltages are applied to the 24 electrostatic lenses. All these voltages are floating on photocathode potential. Intensities of the resulting electron beams are found to be same for both the helicities of light. The polarization of this electron beam is assumed to be 75%.

IV. TARGET PREPARATION

Scattering target is a single crystal Ir(100). This crystal is cleaned *in situ* and Fe is grown on the crystal at the scattering position using an e-beam evaporator without an additional deposition chamber or load lock system.

A. Cleaning the iridium(100) surface

SPLEED is a very surface sensitive technique, since the penetration depth of low energy electron beam inside a crystal is of the order of a few atomic layers. So the surface has to be very clean. The main contamination in Ir(100) single crystal is carbon, which is confirmed by AES. Carbon at the surface is removed by oxidising it to carbon monoxide (CO), which is pumped by UHV pumps.[18,24] UHP oxygen is introduced into the scattering chamber so that the pressure in the chamber becomes 5×10^{-8} mbar. A high voltage of 1.25 kV is applied to the crystal with respect to ground and a current is passed through the grounded filament to form 71 mA emission current to the crystal, which gives around 89 W power. Filament is kept on for 13 s for the cathode to get heated up to 1000 °C, and the carbon at the surface then reacts with oxygen to form

CO. Following this, it is kept off for 47 s, and during this time the oxygen gets adsorbed to the surface.[24] This cycle is repeated 15 times. During this process, carbon in the bulk of the crystal diffuses to the surface and gets oxidised and desorbed. Thermal desorption spectroscopy by using quadrupole mass spectrometer confirms the formation and removal of the CO. AES spectrum shows no carbon peak after 15 cycles of cleaning. During this process, iridium oxide forms at the surface. Iridium oxide and atomic oxygen are removed by giving a high temperature flash up to 1200 °C in UHV, by applying 1.25 kV to crystal, and passing a current through filament to form 120 mA emission current, which gives 150 W power.[12,18,25,26] Oxygen removal is confirmed by AES.

Heating the Ir(100) crystal above 800 K leads to a 1×5 reconstruction at the surface, which is evident from LEED images. This 1×5 reconstructed surface is brought back to 1×1 unreconstructed surface by oxygen and hydrogen treatment.[25] LEED images of 1×5 Ir(100), 1×1 Ir(100), and 5 ML Fe deposited on 1×1 Ir(100) taken at 100 eV are shown in Figure 4.

B. Iron deposition on iridium(100)

The growth of Fe on Ir(100) is pseudomorphic up to 10 monolayer (ML) and gradually relaxes to BCC Fe(100) beyond that thickness.[27] Using an e-beam evaporator, Fe(100) is grown on Ir(100). The growth is monitored using MEED oscillations. For this a 3 keV electron beam is incident at a grazing angle of 2.5° on the crystal and the reflected electrons are counted using MCP. The oscillation of electron counts, with respect to Fe evaporation, gives the information about the growth of Fe; the growth is layer by layer and the oscillations are obtained up to 20 ML.

The scattering experiment is performed at the two remanent states of the ferromagnetic film in order to extract the asymmetry due to spin-orbit and exchange interaction. For this, the sample has to be magnetized parallel and antiparallel to the spin quantisation axis. Here, we use a current pulse to generate the magnetic field. A five turn coil of diameter 25 mm is inserted below the Ir(100) crystal. The discharge from a capacitor bank is used to produce a current pulse through this coil. Further a magnetic field of 150 Oe is used for magnetizing the Fe(100) films; magnetization is switched from a parallel state to an antiparallel state by changing the direction of the current pulse.

We use only one substrate crystal for different experiments. So, Fe film has to be removed from the substrate for depositing different thicknesses and repeating the experiments. Fe(100) films are removed by flashing above 1000 °C and then substrate is used for next deposition. The flashing is done by applying a voltage of 1.25 kV to the sample and passing a current through the filament kept behind the sample to form 80 mA emission current, which gives 100 W power. Removal of Fe is confirmed by AES.

V. SCATTERING EXPERIMENT

The scattering plane is defined by the wave vector of incident electron, scattering target surface normal, and the scattered electron wave vector. Crystal is mounted in such a way that the scattering plane coincides with the mirror plane of the semi-infinite crystal,[4,26] so that the asymmetry vector is perpendicular to the scattering plane. I_0 is the spin averaged incident electron intensity and I is the spin averaged intensity of (00) reflected beam; $I^{\uparrow}$ is the scattered intensity for the incident spin up electron, and $I^{\downarrow}$ the scattered intensity for the incident spin down electron at a particular angle and energy. Then, the asymmetry is defined as[4]

$$A = (I^{\uparrow} - I^{\downarrow})/(I^{\uparrow} + I^{\downarrow}). \quad (1)$$

Figure of merit is defined as

$$F = S^2(I/I_0), \quad (2)$$

where S is the Sherman function, defined as

$$S = A/P_0, \quad (3)$$

where P_0 is the polarization of incident beam.

At a fixed scattering angle and fixed energy, the specularly reflected electron counts per second are recorded for an incident spin up electron beam by using the MCP. A pulse counter is used to count the number of pulses coming at the anode of the MCP. Then, at the same scattering angle and energy, the specular reflected electron counts per second are recorded for an incident spin down electron beam. Asymmetry is calculated using Equation (1). To avoid the error due to drift and the statistical error, the above process is repeated and the counts are integrated. This process is repeated for different angles and energies.

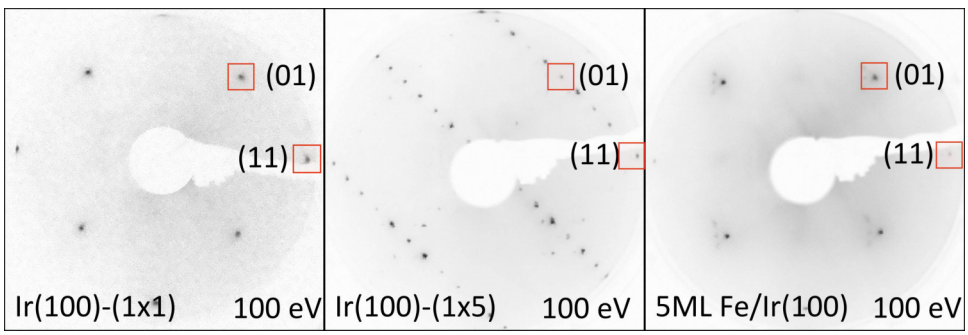

FIG. 4. LEED images of 1×1-Ir(100), 1×5-Ir(100), and 5 ML Fe on 1×1-Ir(100) at 100 eV. (01) and (11) spots are shown in boxes.

For a ferromagnetic material, the difference in asymmetries from up magnetized and down magnetized sample will give the asymmetry due to exchange interaction and the average of this asymmetry gives the asymmetry due to spin-orbit interaction.[4] A current pulse is applied through magnetizing coil to magnetize the sample in the upward direction and asymmetry ($A^{\uparrow}$) is recorded as a function of energy. Then a current pulse of opposite sign is applied to magnetize in the downward direction. Again, asymmetry ($A^{\downarrow}$) is recorded in the same energy window. From the two asymmetries, exchange and spin-orbit asymmetries are extracted using[4]

$$\text{asymmetry due to exchange interaction } A_{ex} = (A^{\uparrow} - A^{\downarrow})/2 \tag{4}$$

and

$$\text{asymmetry due to spin-orbit interaction } A_{so} = (A^{\uparrow} + A^{\downarrow})/2. \tag{5}$$

VI. RESULT AND DISCUSSION

Iridium is a non-ferromagnetic high Z material, and the asymmetry arises from spin-orbit interaction as in the case of tungsten and gold.[12,26,28] The scattered count and asymmetry vs energy plot from a 1×5 Ir(100) are shown in Fig. 5 at a fixed angle of incidence of 45°. The energy is varied from 10 eV to 100 eV. Even though the angle of incidence can be varied continuously between 10° and 85°, we present the data for 45° just to demonstrate the capability of this instrument. In Fig. 5(a), the filled upward triangle is the reflected intensity for an incident spin up electron beam and the empty downward triangle is the reflected intensity for an incident spin down electron beam. Fig. 5(b) shows the asymmetry. Asymmetry has a maximum value of 37.7% ± 0.2% at 42 eV. Error bars are of the size of the symbol. The asymmetry profile agrees fairly well with the asymmetry reported by Kutnyakhov *et al.*[26] Even in the UHV condition the Ir(100) surface remains clean only for a few hours. Hence, the complete evaluation of angle and energy dependence of figure of merit is tedious. Therefore, the Ir(100) surface is passivated with oxygen or hydrogen, which showed stability for several days. We have evaluated the figure of merit for these surface configurations. The maximum figure of merit obtained for oxygen passivated Ir(100) surface is 8×10^{-4} at 29 eV and at an angle of incidence of 15°.

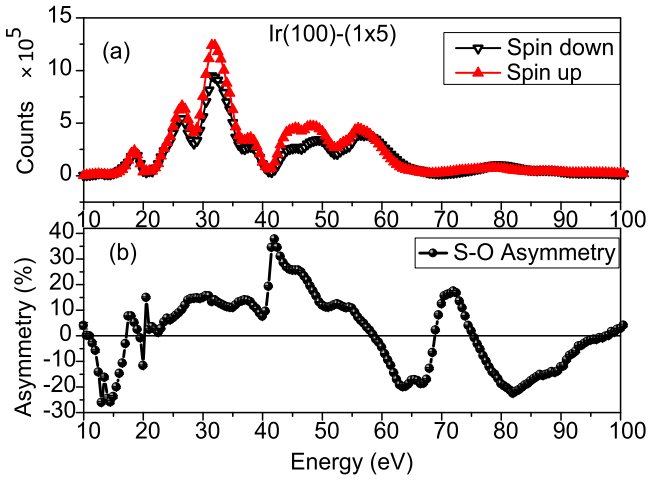

FIG. 5. (a) Reflected electron count and (b) asymmetry from clean 1×5 Ir(100) at 45° angle of incidence.

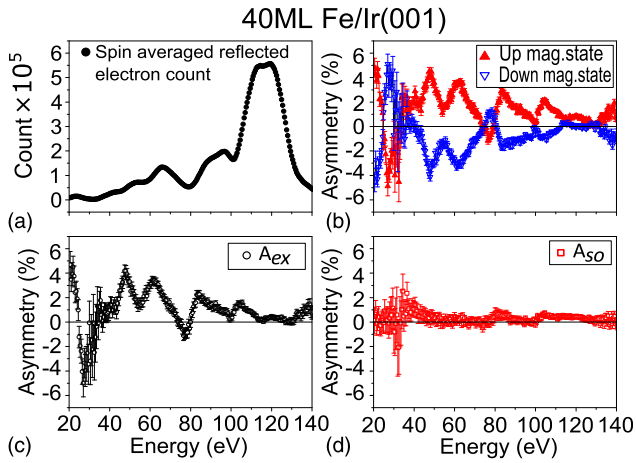

FIG. 6. (a) Spin averaged reflected electron count, (b) asymmetry from up magnetized (red filled triangle) and down magnetized (blue down pointing triangle) 40 ML Fe on 1×1 Ir(100), (c) exchange asymmetry, and (d) spin-orbit asymmetry, as a function of energy, at 45° angle of incidence.

Fe films should show asymmetry due to exchange interaction, since it is a ferromagnetic material, as well as spin orbit interactions. However, the asymmetry due to spin-orbit interaction is weak, because of low atomic number. There is no exchange asymmetry observed from 1 to 4 ML Fe films. But exchange asymmetries are observed from Fe films thicker than or equal to 5 ML. Exchange asymmetries from Fe(001)-p(1 × 1)O have been reported recently over a wide range of scattering angle and over an energy range different from our energy range.[29] Figs. 6(a)-6(d) show the spin averaged reflected electron count, asymmetry of up magnetized state, asymmetry of down magnetized state, exchange asymmetry, and spin orbit asymmetry, respectively, from 40 ML equivalent of Fe on 1×1 Ir(100). In Fig. 6(b), the filled upward triangle is the asymmetry from up magnetized sample, and the empty downward triangle is the asymmetry from the down magnetized sample. In most of the region, the asymmetry flips sign with the magnetization giving rise to an almost zero spin-orbit asymmetry.

VII. CONCLUSIONS

We have designed and fabricated a spin polarized low energy diffraction system in UHV. Focussing voltages are optimized to get well collimated spin polarized electron beam in a wide energy range with high intensity. An asymmetry of 37.7% ± 0.2% at 42 eV energy is obtained for 1×5 Ir(100). The easiness of cleaning in UHV and large asymmetry make iridium a good candidate for spin polarimeter. An exchange asymmetry of 4.2% ± 0.5% at 48.5 eV is obtained from 40 ML of Fe(100)/Ir(100). Fe films can be easily removed from Ir(100) by flashing and then new film can be deposited. This gives promises in the direction of electron spin polarimeter based on exchange scattering from Fe films as well.

ACKNOWLEDGMENTS

The authors are thankful to the Max-Planck Society for the financial support. P. S. Anil Kumar thanks Max-Planck Society for the Max-Planck partner group grant. A.V.P. and A.R. thank Council for Scientific and Industrial Research (CSIR), India for financial support.

[1]J. Kessler, *Polarized Electrons* (Springer, Berlin, Heidelberg, 1976).
[2]V. Guidi, Hyperfine Interact. **127**, 455 (2000).
[3]H. Batelaan, T. J. Gay, and J. J. Schwendiman, Phys. Rev. Lett. **79**, 4517 (1997).
[4]R. Feder, *Polarized Electrons in Surface Physics* (World Scientific, Singapore, 1985).
[5]S. Suga and C. Tusche, J. Electron Spectrosc. Relat. Phenom. **200**, 119 (2015).
[6]D. Yu, C. Math, M. Meier, M. Escher, G. Rangelov, and M. Donath, Surf. Sci. **601**, 5803 (2007).
[7]T. Okuda, Y. Takeichi, A. Harasawa, I. Matsuda, T. Kinoshita, and A. Kakizaki, Eur. Phys. J.: Spec. Top. **169**, 181 (2009).
[8]M. Kolbe, P. Lushchyk, B. Petereit, H. J. Elmers, G. Schönhense, A. Oelsner, C. Tusche, and J. Kirschner, Phys. Rev. Lett. **107**, 207601 (2011).
[9]C. Tusche, M. Ellguth, A. A. Ünal, C.-T. Chiang, A. Winkelmann, A. Krasyuk, M. Hahn, G. Schönhense, and J. Kirschner, Appl. Phys. Lett. **99**, 032505 (2011).
[10]A. Winkelmann, D. Hartung, H. Engelhard, C.-T. Chiang, and J. Kirschner, Rev. Sci. Instrum. **79**, 083303 (2008).
[11]T. Okuda, Y. Takeichi, Y. Maeda, A. Harasawa, I. Matsuda, T. Kinoshita, and A. Kakizaki, Rev. Sci. Instrum. **79**, 123117 (2008).
[12]J. Kirschner, F. Giebels, H. Gollisch, and R. Feder, Phys. Rev. B **88**, 125419 (2013).
[13]R. Feder, Solid State Commun. **31**, 821 (1979).
[14]B. Ackermann and R. Feder, Solid State Commun. **49**, 489 (1984).
[15]M. S. Hammond, G. Fahsold, and J. Kirschner, Phys. Rev. B **45**, 6131 (1992).
[16]U. Gradmann, G. Waller, R. Feder, and E. Tamura, J. Magn. Magn. Mater. **31-34**, 883 (1983).
[17]P. Drescher, H. G. Andresen, K. Aulenbacher, J. Bermuth, T. Dombol, H. Fischerz, H. Euteneuer, N. N. Faleev, M. S. Galaktionov, D. Harrach, P. Hartmann, J. Hoffmann, P. Jennewein, K. H. Kaiser, S. Köbis, O. V. Kovalenkov, H. J. Kreide, J. Langbeine, Y. A. Mamaev, C. Nachtigall, M. Petri, S. Plützer, E. Reicherte, M. Schemies, H.-J. Schöpe, K.-H. Steffens, M. Steigerwald, A. V. Subashiev, H. Trautner, D. A. Vinokurov, Y. P. Yashin, and B. S. Yavich, Appl. Phys. A: Mater. Sci. Process. **63**, 203 (1996).
[18]R. G. Musket, W. McLean, C. A. Colmenares, D. M. Makowiecki, and W. J. Siekhaus, Appl. Surf. Sci. **10**, 143 (1982).
[19]D. T. Pierce and F. Meier, Phys. Rev. B **13**, 5484 (1976).
[20]D. T. Pierce, R. J. Celotta, G.-C. Wang, W. N. Unertl, A. Galejs, C. E. Kuyatt, and S. R. Mielczarek, Rev. Sci. Instrum. **51**, 478 (1980).
[21]R. Cun-Jun, Chin. Phys. **12**, 483 (2003).
[22]T. Maruyama, E. L. Garwin, R. Prepost, G. H. Zapalac, J. S. Smith, and J. D. Walker, Phys. Rev. Lett. **66**, 2376 (1991).
[23]R. Calabrese, G. Ciullo, V. Guidi, G. Lamanna, P. Lenisa, B. Maciga, L. Tecchio, and B. Yang, Rev. Sci. Instrum. **65**, 343 (1994).
[24]K. Zakeri, T. R. F. Peixoto, Y. Zhang, J. Prokop, and J. Kirschner, Surf. Sci. **604**, L1 (2010).
[25]K. Heinz, G. Schmidt, L. Hammer, and K. Müller, Phys. Rev. B **32**, 6214 (1985).
[26]D. Kutnyakhov, P. Lushchyk, A. Fognini, D. Perriard, M. Kolbe, K. Medjanik, E. Fedchenko, S. A. Nepijko, H. J. Elmers, G. Salvatella, C. Stieger, R. Gort, T. Bähler, T. Michlmayer, Y. Acremann, A. Vaterlaus, F. Giebels, H. Gollisch, R. Feder, C. Tusche, A. Krasyuk, J. Kirschner, and G. Schönhense, Ultramicroscopy **130**, 63 (2013).
[27]V. Martin, W. Meyer, C. Giovanardi, L. Hammer, K. Heinz, Z. Tian, D. Sander, and J. Kirschner, Phys. Rev. B **76**, 205418 (2007).
[28]D. Kutnyakhov, H. J. Elmers, G. Schönhense, C. Tusche, S. Borek, J. Braun, J. Minár, and H. Ebert, Phys. Rev. B **91**, 014416 (2015).
[29]C. Thiede, C. Langenkämper, K. Shirai, A. B. Schmidt, T. Okuda, and M. Donath, Phys. Rev. Appl. **1**, 054003 (2014).